ELSEVIER

Journal of Nuclear Materials 294 (2001) 104–111

journal of nuclear materials

www.elsevier.nl/locate/jnucmat

Thermodynamics of $(Mg, Ce, U)O_{2+x}(x \gtreqless 0)$ solid solutions

Takeo Fujino [a,*], Kwangheon Park [b], Nobuaki Sato [a], Makoto Yamada [a]

[a] *Institute for Advanced Materials Processing, Tohoku University, 2-1-1 Katahira, Aoba-ku, Sendai 980-8577, Japan*

[b] *Nuclear Reactor Materials Laboratory, Department of Nuclear Engineering, Kyunghee University, Suwon 449-701, South Korea*

Abstract

Quaternary solid solutions, $Mg_yCe_zU_{1-y-z}O_{2+x}(x \gtreqless 0)$, were prepared and equilibrated under various oxygen partial pressures. The solubility of magnesium in $Ce_{0.1}U_{0.9}O_{2+x}$ was about $y = 0.05$, and above this concentration MgO precipitated, forming a two-phase mixture. In $Mg_yCe_zU_{1-y-z}O_{2+x}$ with $y \leqslant 0.05$, a part of the dissolved magnesium atoms occupy the interstitial 4*b* position of $Fm\bar{3}m$. The ratio of the interstitial magnesium to the total magnesium increases from about 0.3 to 0.6 as the oxygen partial pressure decreases to 10^{-19}–10^{-21} atm. The rates of change of the lattice parameter, $\partial a/\partial y$, $\partial a/\partial z$ and $\partial a/\partial x$, for x greater than 0 were somewhat smaller in absolute values than literature values. For $x < 0$, the rates $\partial a/\partial z$ and $\partial a/\partial x$ were in good agreement with the literature values. However, $\partial a/\partial y$ was much smaller as absolute value due to interstitial magnesium. A plot of oxygen potential vs O/M ratio at 1000°C showed a marked shift to lower x for the $Mg_yCe_zU_{1-y-z}O_{2+x}$ solid solution. The shift rate was −0.01 per 1 mol% magnesium. © 2001 Elsevier Science B.V. All rights reserved.

PACS: 28.41.Bm

1. Introduction

Thermodynamic properties of $CeO_2 - UO_2$ solid solution, denoted as $Ce_zU_{1-z}O_{2+x}(x \gtreqless 0)$, have been studied by a number of researchers [1–5]. With increasing concentration of cerium, this solid solution widens its oxygen non-stoichiometric region of existence into extended hypostoichiometry. The oxygen potential, $\Delta\overline{G}_{O_2}$, of the solid solution decreases more slowly as the O/M ratio (M = Ce + U) of the solid solution decreases [6–9]. The thermodynamic properties of the cerium solid solution are thought to be close to those of PuO_2–UO_2 solid solution (MOX) due to similar physico-chemical properties of cerium and plutonium. For this reason, cerium solid solutions are often used as a stand-in for studying the irradiation behavior of MOX fuel.

No reports on the thermodynamic properties of quaternary solid solution, $Mg_yCe_zU_{1-y-z}O_{2+x}(x \gtreqless 0)$ have been found. $Mg_yU_{1-y}O_{2+x}$ solid solution shows peculiar thermodynamic properties, viz. the curve of oxygen potential vs O/M ratio plot shifts to lower O/M ratio with increasing magnesium concentration in contrast to the usual solid solutions [10–12]. Also, doping of magnesium in UO_2 produced larger grain sized pellets than for undoped UO_2 pellets [13]. The fission gas release rate of the magnesium doped UO_2 fuel with larger grain size was significantly reduced when the fuel was irradiated in light water reactors [13–15]. If the above effect also occurs for magnesium doped MOX, better fuel performance during irradiation would be obtained. The thermodynamic properties of MOX fuel can be estimated by examining $Mg_yCe_zU_{1-y-z}O_{2+x}$, the study of which is important also from the viewpoint of basic solid solution chemistry.

In this work, $Mg_yCe_zU_{1-y-z}O_{2+x}$ solid solutions were prepared under various heating conditions. The $MgO - Ce_zU_{1-z}O_{2+x}$ phase relations as well as the solubility and crystallographic position of magnesium in the solid solution were studied. Oxygen potential measurements were carried out, and compared with those of other solid solutions.

* Corresponding author. Tel.: +81-22 217 5163; fax: +81-22 217 5164.

E-mail address: fujino@iamp.tohoku.ac.jp (T. Fujino).

PII: S0022-3115(01)00452-4

2. Experimental

2.1. Materials used

Uranium was purified as follows: The metal turnings were dissolved in 6 M nitric acid, and the uranium was extracted from the aqueous solution into TBP. The uranium was scrubbed with water and then with dilute ammonium carbonate solution. Ammonium diuranate precipitate, which was formed by adding ammonium hydroxide to the purified uranium solution, was filtered off, dried and subsequently converted to UO_3 by heating in air at 500°C [16]. Stoichiometric UO_2 was obtained by heating UO_3 in a stream of H_2 at 1000°C for 6 h.

Guaranteed reagent heavy MgO (CaO < 0.05%, heavy metal < 0.005%) was purchased from Wako Pure Chemicals Industries. Cerium dioxide of 99.9% purity was obtained from Michigan Chemical. High purity hydrogen gas was produced by a Whatman Model 75-34JA-100 generator. Carbon dioxide and N_2 (99.999%) gases were obtained from Nippon Sanso and used as received.

2.2. Preparation of solid solutions

The calculated amounts of MgO, CeO_2 and UO_2 were intimately mixed in an agate mortar for about 40 min. The mixture was heated in air in a muffle furnace at 800°C for 3 days to create higher oxides. The cycle of mixing and heating was repeated three times to obtain the well-mixed oxides.

About 1 g of the air heated oxide was pressed into a pellet of 10 mm diameter. Several pellets were heated together on an alumina boat in a horizontal SiC resistance tube furnace at 1200°C for 2 days in a stream of CO_2. After the reaction, the pellets were crushed and ground. The powder was again pelletized and heated under the same conditions. This cycle was repeated three times.

Equilibration experiments were carried out to study the effect of oxygen partial pressure. In order to attain equilibrium, the solid solution pellets were heated in the SiC tube furnace for 3 days in a stream of CO_2/H_2 gas of which the mixing ratio was controlled with two mass-flow controllers (Kofloc, Type-3510 1/4SW-500SCCM and 1/4-10SCCM).

2.3. X-ray diffraction analysis

X-ray powder diffractometry was performed with a Rigaku RAD-IC diffractometer using CuKα radiation (40 kV, 20 mA) monochromatized with curved pyrolytic graphite. The slit system used was 1°–0.5 mm–1°–0.15 mm. The ratemeter measurement was made in a 2θ range between 10° and 140° with a scanning rate of $1°(2\theta)$ per min. The lattice parameter of the cubic solid solution was calculated by the least-squares method using the LCR2 program [17]. The precipitation of MgO phase from the solid solution was checked by step scanning measurement (18 s counting time and $0.01°(2\theta)$ step width) in a range $40.88° \leqslant 2\theta \leqslant 44.88°$ to detect the strongest diffraction peak of MgO at 42.8°.

2.4. Chemical analysis

Ten to 20 mg of solid solution powder was weighed with an accuracy of ±10 μg. The sample was dissolved in 5 ml of 0.05 M Ce(IV) solution in 1.5 M sulfuric acid by warming the solution to 80–90°C. The O/M ratio of the solid solution was determined by titrating the amount of excess Ce(IV) with Fe(II) ammonium sulfate solution using ferroin indicator [18,19]. The concentrations of Ce(IV) and Fe(II) solutions used were standardized by titration using stoichiometric UO_2 freshly reduced by heating in H_2. The estimated standard deviation in the measured O/M ratios was within ±0.005.

2.5. Density measurement

The density of solid solutions was measured by the toluene displacement method. The sample powder of 1.5–3 g was precisely weighed in a small glass bulb of 7.4243 g first in air and then in toluene at 20°C. The bulb containing the sample was evacuated by rotary pump in a desiccator until no bubbles from the open pores were formed. The error in the densities determined by this method was estimated to be within ±0.1 g/cm^3.

2.6. Oxygen potential measurement

The solid solution sample of about 400 mg in a quartz basket was precisely weighed and then suspended with platinum wire from a Cahn D-200 digital recording electrobalance. After evacuating for 1 h, the vacuum system was closed, and no leakage of vacuum was checked for several hours on a mercury manometer. Nitrogen gas was introduced up to the ambient pressure, and then the mixed gas of CO_2/H_2, controlled by the two mass flow controllers, was passed over the sample. Subsequently, the furnace temperature was raised to the intended temperature, and the sample weight was measured after the sample had equilibrated with the oxygen partial pressure, as determined by monitoring the rate of weight-change. The oxygen partial pressure and hence $\Delta\overline{G}_{O_2}(= RT\ln p_{O_2})$ of this sample, with known O/M ratio by thermogravimetry, were calculated from the CO_2/H_2 ratio by the use of the literature ΔG° values for $H_2O(g), CO_2(g)$ and CO(g) [20]. Below oxygen partial pressures of 10^{-15} atm, nickel wire was used to suspend the sample from the electrobalance.

3. Results and discussion

3.1. Solid solutions in high oxygen partial pressures

All samples prepared in this work ($0.03 \leqslant y \leqslant 0.1$, $z = 0.05$ and 0.1) in the CO_2 stream at 1200°C (oxygen partial pressure: 3.13×10^{-4} atm) gave sharp diffraction lines in the X-ray diffraction patterns showing good crystallinity of the samples. They were single-phase solid solutions as confirmed by the X-ray step scanning measurements in the 2θ range from 40.88° to 44.88° where no MgO peak was detected. This result that magnesium was soluble in cerium solid solutions above $y = 0.1$ accords with the behavior of magnesium solid solution, $Mg_yU_{1-y}O_{2+x}$, where the magnesium solubility increases with increasing oxygen pressure in the range over 10^{-6} atm approaching the maximum magnesium solubility of $y = 1/3$ [21,22]. Table 1 shows the lattice parameters and compositions determined by chemical analysis of the solid solutions. In order to obtain an equation that represents the lattice parameter change in the $x > 0$ region due to changes in y, z and x of $Mg_yCe_zU_{1-y-z}O_{2+x}$, the rates of $\partial a/\partial y$ and $\partial a/\partial z$ were calculated for a selected value of $\partial a/\partial x$ using the three pairs of lattice parameter-composition data for $z = 0.05$ in Table 1. This $\partial a/\partial x$ value was varied, and the best fit of a (calc) to a (obs), was obtained at $\partial a/\partial x = -0.095$. The modified lattice parameters for oxygen stoichiometry, i.e., $Mg_yCe_{0.05}U_{0.95-y}O_2$, were calculated by using this $\partial a/\partial x$ value. They are plotted in Fig. 1 as a function of y value. From the slope of the straight line connecting these points, the rate, $\partial a/\partial y$, was obtained as -0.48. From the lattice parameter at $y = 0$, viz. 5.4686 Å, the factor $\partial a/\partial z$ was obtained as -0.04 with the use of 5.4704 Å as the lattice parameter for stoichiometric UO_2 [23]. The lattice parameter change is thus

$$a = 5.4704 - 0.48y - 0.04z - 0.095x. \quad (1)$$

The lattice parameters calculated by using this equation are listed in Table 1 as a (calc). Magnesium atoms are considered to occupy substitutional sites at these high oxygen partial pressures [22]. Cerium atoms in all cases occupy the substitutional sites. The literature rates are $\partial a/\partial y = -0.546 \sim -0.568, \partial a/\partial z = -0.057 \sim -0.067$ and $\partial a/\partial x = -0.102 \sim -0.14$ [21]. The rates obtained in this work are seen to be somewhat smaller as absolute values. As a possible reason for this difference, stronger interaction between the defects in this quaternary solid solution is postulated.

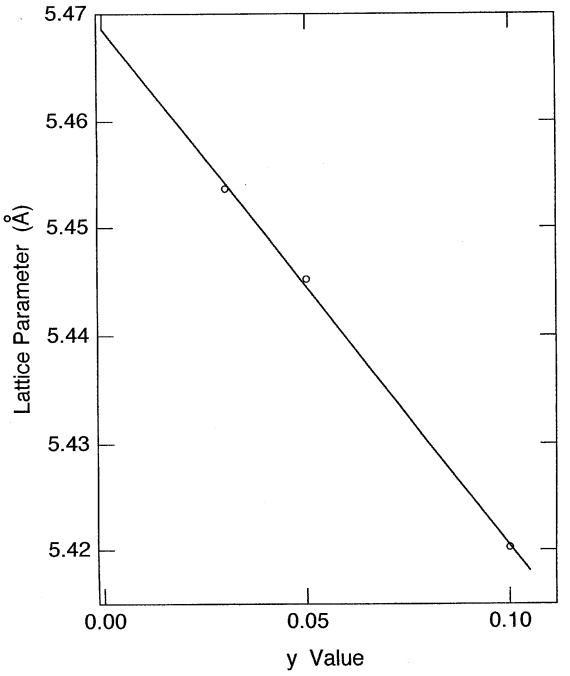

Fig. 1. Lattice parameter of stoichiometric solid solution, $Mg_yCe_{0.05}U_{0.95-y}O_2$, as a function of y. Heating temperature: 1200°C; atmosphere: high oxygen partial pressure of 3.13×10^{-4} atm.

3.2. Solid solutions in low oxygen partial pressures

3.2.1. Phase relations

A series of equilibration experiments were carried out for the five heating conditions shown in Table 2. The X-ray diffraction step scanning measurements for $2\theta = 40.88$–$44.88°$ showed that MgO had precipitated in all the $y = 0.1, z = 0.1$ samples of the five heating conditions. Figs. 2 ((a) and (c)) show the patterns for $y = 0.05$ at 8.8×10^{-16} atm O_2 (1050°C) and at 10^{-19}–10^{-21} atm O_2 (1200°C), respectively. For the magnesium concentration of $y = 0.05$, no MgO peaks are detected. The patterns of Figs. 2 ((b) and (d)) are those for the samples of $y = 0.1$ at 8.8×10^{-16} atm O_2 (1050°C) and at $10^{-19} \sim 10^{-21}$ atm O_2

Table 1
Compositions and lattice parameters for $Mg_yCe_zU_{1-y-z}O_{2+x}$ solid solutions prepared in a high oxygen partial pressure of CO_2 gas at 1200°C

Solid solution	$y = 0.03,\ z = 0.05$	$y = 0.03,\ z = 0.1$	$y = 0.05,\ z = 0.05$	$y = 0.1,\ z = 0.05$
x value (O/M-2)	0.153 ± 0.001	0.142 ± 0.002	0.134 ± 0.004	0.090 ± 0.002
a (obs) (Å)	5.4391 ± 0.0001	5.4414 ± 0.0001	5.4325 ± 0.0002	5.4117 ± 0.0001
a (calc) (Å)	5.4395	5.4385	5.4317	5.4119

Table 2
O/M ratios, lattice parameters and observed densities after equilibration experiments

No.	Sample heating condition	$y = 0, z = 0.1$	$y = 0.05, z = 0.1$	$y = 0.1, z = 0.1$
1	1050°C $p(O_2) = 8.8 \times 10^{-16}$ atm $\Delta\overline{G}_{O_2} = -381.3$ kJ/mol	O/M = 1.991 $a = 5.4650$ Å $d = 10.40$ g/cm^3	O/M = 1.959 $a = 5.4570$ Å $d = 10.23$ g/cm^3	O/M = 1.912 $a = 5.4572$ Å[a] $d = 9.98$ g/cm^3
2	1200°C $p(O_2) = 5.3 \times 10^{-8}$ atm $\Delta\overline{G}_{O_2} = -205.2$ kJ/mol	O/M = 2.006 $a = 5.4643$Å	O/M = 1.996 $a = 5.4509$ Å	O/M = 1.944 $a = 5.4613$ Å[b]
3	1200°C $p(O_2) = 2.0 \times 10^{-14}$ atm $\Delta\overline{G}_{O_2} = -386.3$ kJ/mol	O/M = 1.999 $a = 5.4650$ Å $d = 10.37$ g/cm^3	O/M = 1.958 $a = 5.4589$ Å $d = 10.28$ g/cm^3	O/M = 1.908 $a = 5.4589$ Å[a] $d = 9.88$ g/cm^3
4	1200°C $p(O_2) = 10^{-19} \sim 10^{-21}$ atm $\Delta\overline{G}_{O_2} = -535 \sim -592$ kJ/mol	O/M = 1.993 $a = 5.4656$ Å $d = 9.92$ g/cm^3	O/M = 1.935 $a = 5.4647$ Å $d = 10.04$ g/cm^3	O/M = 1.889 $a = 5.4635$ Å[a] $d = 10.02$ g/cm^3
5	1200°C $p(O_2) = 10^{-19} \sim 10^{-21}$ atm $\Delta\overline{G}_{O_2} = -535 \sim -592$ kJ/mol	O/M = 1.989 $a = 5.4654$ Å $d = 10.39$ g/cm^3	O/M = 1.955 $a = 5.4644$ Å $d = 10.08$ g/cm^3	O/M = 1.901 $a = 5.4646$ Å[a] $d = 9.92$ g/cm^3

[a] MgO + fluorite phase.
[b] MgO + two fluorite phases. Fluorite lattice parameter is for the phase with stronger peaks.

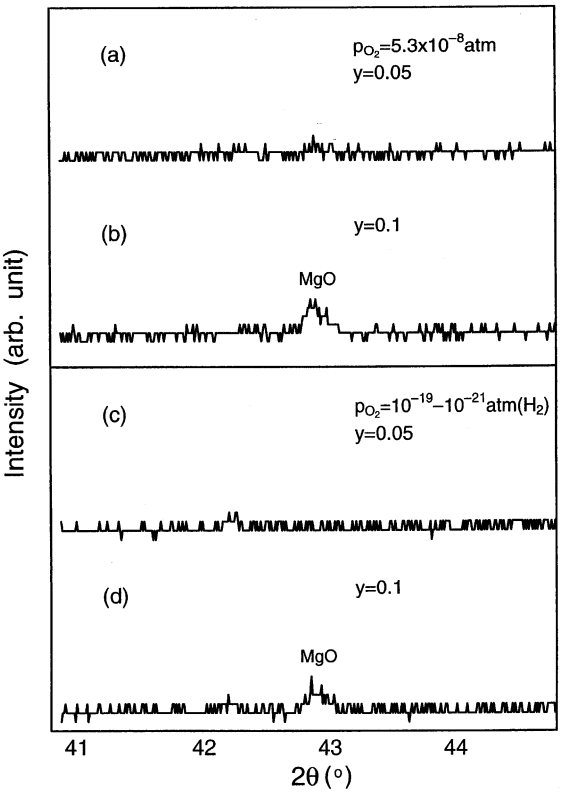

Fig. 2. Step scanned X-ray diffraction patterns for the samples of two magnesium concentrations in $Mg_yCe_zU_{1-y-z}O_{2+x}$. Cerium concentration: $z = 0.1$; heating temperature: 1200°C. (a) $p_{O_2} = 5.3 \times 10^{-8}$ atm, $y = 0.05$; (b) $p_{O_2} = 5.3 \times 10^{-8}$ atm, $y = 0.1$; (c) $p_{O_2} = 10^{-19}$–10^{-21} atm, $y = 0.05$; (d) $p_{O_2} = 10^{-19}$–10^{-21} atm, $y = 0.1$.

(1200°C), respectively, in which the strongest peaks of MgO are observed to emerge at about 42.8°. The peak intensity in Fig. 2(b) is higher than that in Fig. 2(d). The phase separation at $y = 0.1$ is also observed in the lattice parameter change with y value as shown in Fig. 3. In the regions of y values where the lattice parameter did not change with y value, the phase consists of the mixture of MgO and solid solution. This figure suggests that magnesium dissolves in the host cerium solid solution with the concentration slowly increasing with decreasing oxygen partial pressure, i.e., from about $y = 0.045$ at 8.8×10^{-16} atm O_2 (1050°C) to about 0.065 at 10^{-19}–10^{-21} atm O_2 (1200°C). The magnesium solubility in this solid solution is, however, lower than those in undoped UO_2 [10] and gadolinium solid solutions [23], where the solubilities exceed $y = 0.1$.

3.2.2. Density of magnesium and cerium doped UO_2

If magnesium atoms occupy partly substitutional sites (4*a* position of space group $Fm\bar{3}m$) and partly interstitial sites (4*b* position), the formula $Mg_yCe_zU_{1-y-z}O_{2+x}$ should be changed to

$$\begin{aligned} &Mg_yCe_zU_{1-y-z}O_{2+x} \\ &\quad \rightarrow (1-my)Mg_{\frac{(1-m)y}{1-my}}Ce_{\frac{z}{1-my}}U_{\frac{1-y-z}{1-my}}\{Mg_{\frac{my}{1-my}}\}O_{\frac{2+x}{1-my}}, \end{aligned} \tag{2}$$

where m stands for the ratio of the interstitial magnesium atoms to the total magnesium atoms. In the right side of the formula above, the sum of magnesium, cerium and uranium atoms in the substitutional sites is one. Wholly substitutional and interstitial solid solutions are expressed by setting $m = 0$ and 1, respectively.

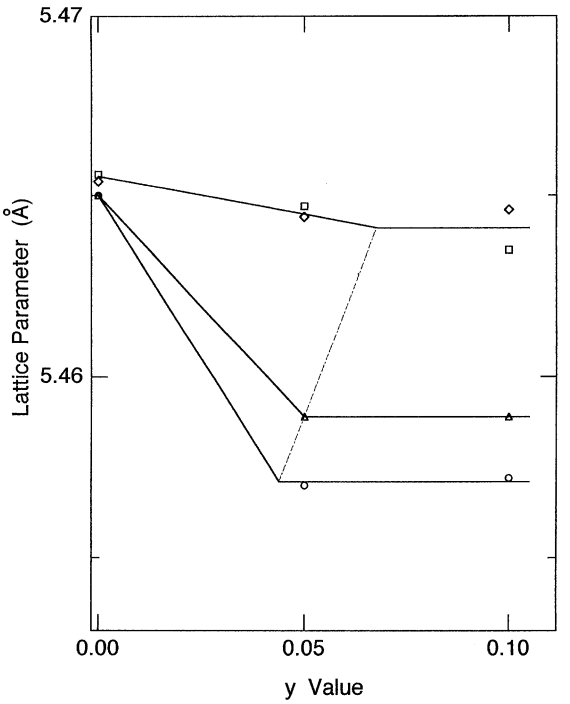

Fig. 3. Lattice parameter change of magnesium doped cerium solid solution heated in low oxygen partial pressures as a function of y. Cerium concentration: $z = 0.1$. (○) $p_{O_2} = 8.8 \times 10^{-16}$ atm (1050°C), No. 1 in Table 2; (△) $p_{O_2} = 2.0 \times 10^{-14}$ atm (1200°C), No. 3 in Table 2; (□) $p_{O_2} = 10^{-19} \sim 10^{-21}$ atm (1200°C), No. 4 in Table 2; (◇) $p_{O_2} = 10^{-19} \sim 10^{-21}$ atm (1200°C), No. 5 in Table 2.

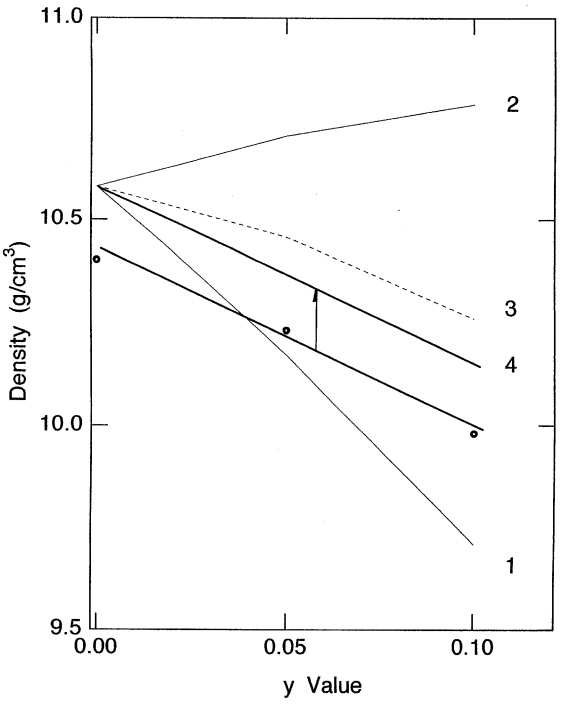

Fig. 4. Pycnometric densities compared with theoretical densities for the samples $Mg_yCe_zU_{1-y-z}O_{2+x}$ heated in $p_{O_2} = 8.8 \times 10^{-16}$ atm at 1050°C. (○) Observed density; (1) theoretical substitutional density; (2) theoretical interstitial density; (3) theoretical mixture density; (4) closed pore corrected observed density.

On the other hand, if the material produced is a mixture of MgO and cerium solid solution, the formula becomes [25]

$$Mg_yCe_zU_{1-y-z}O_{2+x} \rightarrow yMgO + (1-y)Ce_{\frac{z}{1-y}}U_{\frac{1-y-z}{1-y}}O_{2+\frac{x+y}{1-y}}. \quad (3)$$

Eq. (3) is for the case where the quaternary solid solution containing magnesium is not formed. There is a possibility of an intermediate case between Eqs. (2) and (3).

The change of density with magnesium concentration (y) for the samples heated at 1050°C in 8.8×10^{-16} atm O_2 is shown in Fig. 4. The theoretical density was calculated with the composition and lattice parameter. Lines 1 and 2 in the figure show the theoretical densities for substitutional and interstitial magnesium, respectively. Line 3 (broken line) shows the theoretical change for the mixture of MgO and

$$Ce_{\frac{z}{1-y}}U_{\frac{1-y-z}{1-y}}O_{2+\frac{x+y}{1-y}}.$$

Calculation of the density of the mixture was made using 4.2117 Å for the MgO lattice parameter [26] together with the lattice parameter of solid solution and the known bulk composition. In Fig. 4, the observed densities given as circles are low due to the presence of closed pores in the specimens. But the important information is in the slope of the observed densities. The measured density line was translated up so that it agreed with the theoretical density at $y = 0$. This line (line 4) is between those of the substitutional and interstitial solid solutions although it should be noted that the $y = 0.1$ specimen is a two-phase mixture with MgO. From this line, two possibilities remain: one is the case of Eq. (2) with $m = 0.27$ and the other is the case of Eq. (3). The m value was calculated from the slope of line 4.

Fig. 5 shows the densities for the samples equilibrated to 2.0×10^{-14} atm O_2 at 1200°C. A similar result to Fig. 4 was obtained. If magnesium atoms occupy the interstitial sites partly, the m value is 0.34. Densities of the samples heated in an H_2 atmosphere (10^{-19}–10^{-21} atm O_2) at 1200°C shown in Fig. 6 are essentially the same as in Figs. 4 and 5, but the slope is gentler giving $m = 0.68$ if the magnesium atoms partly occupy the interstitial sites. The larger m value in Fig. 6 may be associated with a lower oxygen partial pressure. Such an increase in m at low oxygen partial pressures has

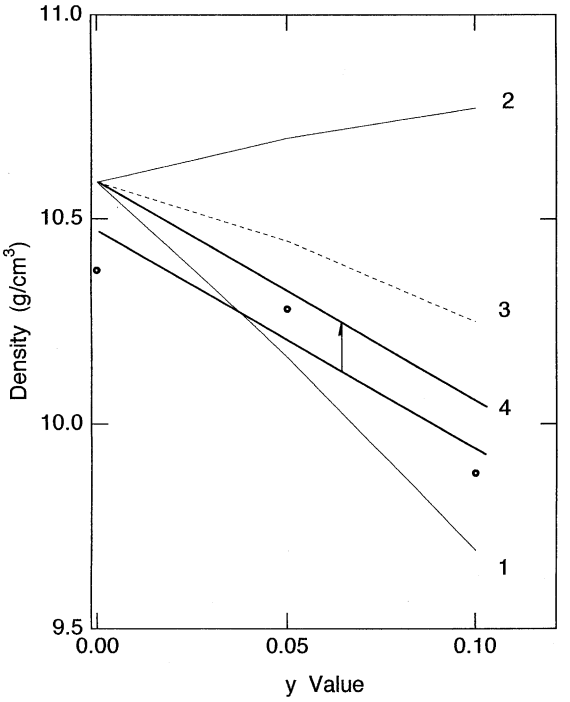

Fig. 5. Pycnometric densities compared with theoretical densities for the samples heated in $p_{O_2} = 2.0 \times 10^{-14}$ atm at 1200°C. (○) Observed density; (1) theoretical substitutional density; (2) theoretical interstitial density; (3) theoretical mixture density; (4) closed pore corrected observed density.

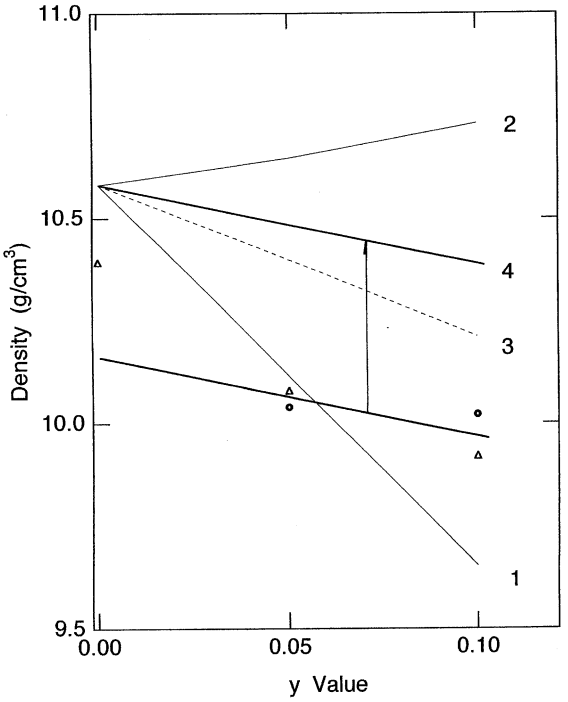

Fig. 6. Pycnometric densities compared with theoretical densities for the samples heated in $p_{O_2} = 10^{-19}$–10^{-21} atm (in a stream of H_2) at 1200°C. (○) Observed density; (1) theoretical substitutional density; (2) theoretical interstitial density; (3) theoretical mixture density; (4) closed pore corrected observed density.

previously been observed for the magnesium solid solution [27]. Density analysis revealed that the possible solid solution should contain magnesium in the interstitial sites. However, definite conclusions on which of Eqs. (2) or (3) is correct cannot be drawn from only the density measurements because the error in the measured densities is not sufficiently small.

3.2.3. Lattice parameter change

In Fig. 7, the lattice parameter is plotted against O/M ratio for $y = 0$, 0.05 and 0.1. The slope of the straight line for cerium solid solution $Ce_zU_{1-z}O_{2+x}$, i.e., $y = 0$, is small giving a rate $\partial a/\partial x = -0.021$. This value is, as absolute value, much smaller than $-0.288 \sim -0.321$ reported for $Ce_zU_{1-z}O_{2+x}$ in the range $x < 0$ by Norris and Kay [9]. At $y = 0.05$, however, the slope increased to $\partial a/\partial x = -0.222$. This value is in agreement with the rate $\partial a/\partial x$ reported for a variety of solid solutions with $x < 0$, although the reference values vary over a wide range (between -0.19 and -0.40) [21]. An important point is that the lines for $y = 0$ and 0.05 are completely different, showing that magnesium dissolves into $Ce_zU_{1-z}O_{2+x}$ up to about $y = 0.05$ forming the quaternary solid solution, $Mg_yCe_zU_{1-z}O_{2+x}$. The lattice parameters for $y = 0.1$ are actually for the solid solutions having y values close to 0.05, namely $Mg_{0.05}Ce_{0.1}U_{0.8}O_{2+x'}$ (or more strictly $Mg_{0.05/0.95}Ce_{0.1/0.95}U_{0.8/0.95}O_{(2+x)'/0.95}$. The O/M ratios $((2+x')/0.95)$ for $y = 0.1$ are smaller than those in Fig. 7 by about 0.05, since $((2+x')/0.95) = (2+x) - 0.05)$ from the equation,

$$Mg_{0.1}Ce_{0.1}U_{0.8}O_{2+x} = 0.05MgO + 0.95Mg_{0.05/0.95}Ce_{0.1/0.95}U_{0.8/0.95}O_{(2+x)'/0.95}.$$

The slightly steeper slope of -0.257 for $y = 0.1$ than -0.222 for $y = 0.05$ in Fig. 7 might be related to this nonstoichiometry change. It is difficult to do close discussion about the slope for the $y = 0.1$ line because of the scatter of the data. In the region of high oxygen partial pressures, magnesium dissolves in the fluorite lattice occupying substitutional sites up to $y = 1/3$. In the region of low oxygen partial pressures, the soluble amount is near $y = 0.05$, where the magnesium atoms partly occupy substitutional sites and partly interstitial sites: The mechanism of dissolution is different, similar to the case of magnesium solid solution without cerium [10].

Using the $\partial a/\partial x$ rate obtained above, the lattice parameter at oxygen stoichiometric point ($x = 0$) was calculated. The lattice parameters obtained are 5.4650 and

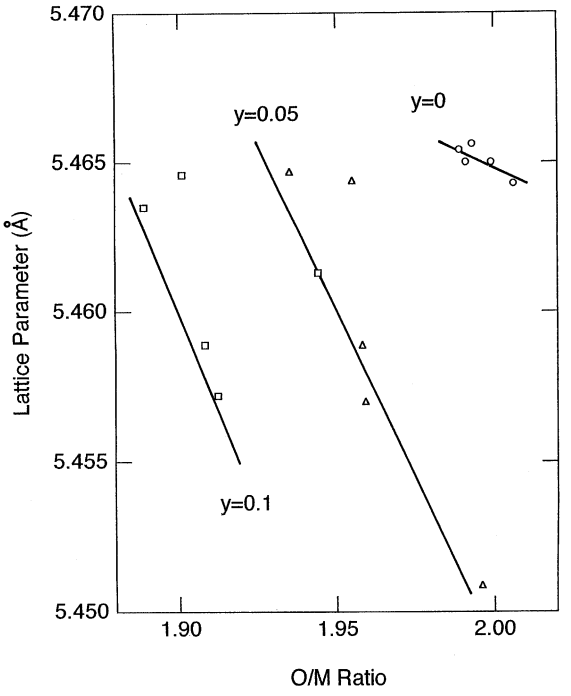

Fig. 7. Lattice parameter of magnesium doped cerium solid solution $Mg_yCe_zU_{1-y-z}O_{2+x}$ ($M = Mg + Ce + U$) heated in low oxygen partial pressures as a function of O/M ratio. Cerium concentration: $z = 0.1$. (○) $y = 0$; (△) $y = 0.05$; (□) $y = 0.1$.

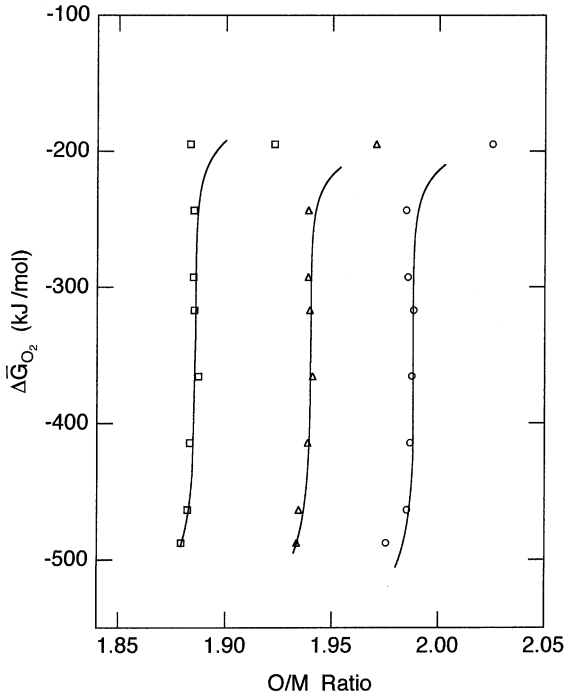

Fig. 8. Oxygen potential of $Mg_yCe_zU_{1-y-z}O_{2+x}$ ($M = Mg + Ce + U$) at 1200°C as a function of O/M ratio. Cerium concentration: $z = 0.1$. (○) $y = 0$; (△) $y = 0.05$; (□) $y = 0.1$.

5.4500 Å as the averages of five equilibration experiments for $y = 0$ and 0.05, respectively. From the linear equation connecting the above two points, i.e., $a = 5.4650 - 0.3y$, the rate $\partial a/\partial z$ is calculated as $(5.4650 - 5.4704)/0.1 = -0.054$. This value is in good agreement with the reference values which are in the range $-0.057 \sim -0.067$ [21]. The rate $\partial a/\partial y$ was calculated to be -0.3 from the slope of the above equation. This rate is much smaller as absolute value than that for high oxygen partial pressures. The difference is considered to be caused by interstitial magnesium in the solid solution. If the $\partial a/\partial y$ rate for interstitial magnesium is +0.29, i.e., the same as that derived for gadolinium solid solution [24], the m value becomes 0.31 which is consistent with those obtained by density measurements (Figs. 4 and 5).

3.3. Oxygen potential

The variation of oxygen potential with O/M ratio of $Mg_yCe_zU_{1-y-z}O_{2+x}$ at 1200°C is shown in Fig. 8 for $y = 0$, 0.05 and 0.1 samples. It is seen that the O/M ratio which gives rise to the steepest change in $\Delta\overline{G}_{O_2}$, which will be referred to as GOM hereafter, shifts leftward if magnesium is added. This shift becomes larger as the magnesium concentration increases. The GOM values are 1.989, 1.940 and 1.886 for $y = 0$, 0.05 and 0.1, respectively. From the difference in GOM for $y = 0$ and 0.05, the rate of shift of GOM was found to be -0.01 (as O/M ratio) per 1 mol% magnesium. The shift due to the increase of y from 0.05 to 0.1 is caused by the precipitation of MgO. Since the $\Delta\overline{G}_{O_2}$ curve for $y = 0.1$ has a very similar shape as that for $y = 0.05$, the 5 mol% MgO in $y = 0.05$ solid solution has almost no effect on $\Delta\overline{G}_{O_2}$ of the solid solution with $y = 0.05$.

Such a shift has already been observed for $Mg_yGd_zU_{1-y-z}O_{2+x}$ solid solution [28,29]. For this solid solution, the rate of shift was $-0.007 \sim -0.008$ [23], which is a little smaller (as absolute value) than the rate of the present solid solution. For $Mg_yGd_zU_{1-y-z}O_{2+x}$, GOM is $2 - \{\alpha(1-m)/2\}y - (1-\beta)z/2$, where α and β are the average composition of the cation complexes with Mg^{2+} and Gd^{3+}, i.e., $(Mg^{2+}\alpha U^{5+})$ and $(Gd^{3+}\beta U^{5+})$, respectively [30]. For the present solid solution also, the corresponding relation is expected to hold.

Acknowledgements

One of the authors, K.P., thanks the Core University Program between Seoul National University and Kyoto

University on Energy Science and Engineering, funded by the Japan Society for the Promotion of Science and the Korea Science and Engineering Foundation for the financial support of his research stay in Japan.

References

[1] M. Hoch, F.J. Furman, in: Thermodynamics, Proceedings of the Symposium 1965, IAEA, Vienna, 1966, vol. 2, p. 517.
[2] R. Lorenzelli, B. Touzelin, J. Nucl. Mater. 95 (1980) 290.
[3] H. Tagawa, T. Fujino, K. Watanabe, Y. Nakagawa, K. Saita, Bull. Chem. Soc. Jpn. 54 (1981) 138.
[4] T. Fujino, J. Nucl. Mater. 154 (1988) 14.
[5] S.H. Kang, H.I. Yoo, H.S. Kim, Y.W. Lee, Korean J. Ceram. 4 (1998) 78.
[6] K. Nagarajan, R. Saha, R.B. Yadav, S. Rajagopalan, K.V.G. Kutty, M. Saibaba, P.R.V. Rao, C.K. Matthews, J. Nucl. Mater. 130 (1985) 242.
[7] T.L. Markin, E.C. Crouch, J. Inorg. Nucl. Chem. 32 (1970) 77.
[8] R. Ducroux, Ph.J. Baptiste, J. Nucl. Mater. 97 (1981) 333.
[9] D.I.R. Norris, P. Kay, J. Nucl. Mater. 116 (1983) 184.
[10] T. Fujino, S. Nakama, N. Sato, K. Yamada, K. Fukuda, H. Serizawa, T. Shiratori, J. Nucl. Mater. 246 (1997) 150.
[11] T. Fujino, N. Sato, J. Nucl. Mater. 189 (1992) 103.
[12] T. Fujino, N. Sato, K. Yamada, J. Nucl. Mater. 223 (1995) 6.
[13] B.E. Ingleby, K. Hand, in: I.J. Hastlings (Ed.), Advances in Ceramics, vol. 17, Fission-Product Behavior in Ceramic Oxide Fuel, American Ceramic Society, Columbus, OH, 1986, p. 57.
[14] P.T. Sawbridge, C. Baker, R.M. Cornell, K.W. Jones, D. Reed, J.B. Ainscough, J. Nucl. Mater. 95 (1980) 119.
[15] S. Kashibe, K. Une, H. Masuda, in: Proceedings of 1996 Spring Meeting of Atomic Energy Society, Japan, Osaka, 27–29 March 1996, K35, p. 521.
[16] H.R. Hoekstra, S. Siegel, E.X. Gallagher, J. Inorg. Nucl. Chem. 32 (1970) 3237.
[17] D.E. Williams, Ames Lab. Rep. IS-1052 (1964).
[18] S.R. Dharwadkar, M.S. Chandrasekharaiah, Anal. Chim. Acta 45 (1969) 545.
[19] T. Fujino, T. Yamashita, Fresenius Z. Anal. Chem. 314 (1983) 156.
[20] DATABASE MALT2, Japanese Society of Calorimetry and Thermal Analysis, 1987.
[21] T. Fujino, C. Miyake, in: A.J. Freeman, C. Keller (Eds.), Handbook on the Physics and Chemistry of the Actinides, vol. 6, North-Holland, Amsterdam, 1991, p. 155.
[22] T. Fujino, J. Tateno, H. Tagawa, J. Solid State Chem. 24 (1978) 11.
[23] H. Nickel, Nukleonik 8 (1966) 366.
[24] T. Fujino, N. Sato, K. Yamada, M. Okazaki, K. Fukuda, H. Serizawa, T. Shiratori, J. Nucl. Mater. 289 (2001) 270.
[25] K. Park, T. Fujino, N. Sato, M. Yamada, in: Proceedings of Autumn Meeting of Korean Nuclear Society, Seoul, October 1999.
[26] B.J. Skinner, Am. Mineral. 42 (1957) 39.
[27] T. Fujino, N. Sato, K. Yamada, J. Nucl. Mater. 247 (1997) 265.
[28] M. Yamada, K. Park, N. Sato, T. Fujino, in: Proceedings of 2000 Spring Meeting of Atomic Energy Society, Japan, Matsuyama, 28–30 March 2000, J50, vol. 3, p. 1028.
[29] T. Fujino, N. Sato, in: Proceedings of 30$^{\text{èmes}}$ Journées des Actinides, Dresden, 4–6 May 2000, p 34.
[30] T. Fujino, N. Sato, J. Nucl. Mater. 282 (2000) 232.